Nanoscale

ARTICLE

Hybrid nanovaccine for co-delivery of mRNA antigen and adjuvant

Jingnan Yang, [a#] Smriti Arya, [b#] Pingsai Lung, [a] Qiubin Lin, [b] Jiandong Huang, [b*] and Quan Li [a*]

For efficient cancer vaccines, antitumor function largely relies on cytotoxic T cells, whose activation can be effectively induced via antigen-encoding mRNA, making mRNA-based cancer vaccines an attractive approach for personalized cancer therapy. While liposome-based delivery system enables the systemic delivery as well as transfection of mRNA, incorporating adjuvant that is non-lipid like remains challenging, although co-delivery of mRNA (antigen) and effective adjuvant is key to the activation of the cytotoxic T cells. This is because the presence of adjuvant is important for dendritic cell maturation—another necessity for cytotoxic T cell activation. In the present work, we designed a poly (lactic-co-glycolic acid) (PLGA)-core/lipid-shell hybrid nanoparticle carrier for the co-delivery of mRNA and gardiquimod (adjuvant that cannot be incorporated into the lipid shell). We demonstrated in the present work that co-delivery of mRNA and gardiquimod led to the effective antigen expression and DC maturation in vitro. Intravenous administration of the hybrid nanovaccine resulted in enrichment of mRNA expression in spleen, and strong immune response in vivo. The simultaneous delivery of antigen and adjuvant both spatially and temporally via the core/shell nanoparticle carrier is found to be beneficial for tumor growth inhibition.

Introduction

Cancer vaccines represent an important branch of cancer immunotherapy. The choice of antigen in cancer vaccine is critical, as it mounts the initial stimulation to the immune system. Among various choices of antigens, mRNA antigen is the most employed one, as it has been found to induce strong major histocompatibility complex (MHC) I-mediated CD8+ T cell (also known as cytotoxic T cell) response, being crucial to bringing antitumor function for personalized cancer vaccine[1, 2]. However, effective mRNA delivery is not an easy task. Intracellular transfection of mRNA to effective antigen is a pre-requisite for antigen presentation in dendritic cells (DCs)[3]. The negative charge of mRNA and lack of targeting function make it difficult for its cellular uptake[2]. Moreover, the easy degradation of mRNA by ubiquitous nucleases limits the methods of administration *in vivo*[2, 3]. In most cases, systemic mRNA delivery using intravenous (i.v.) administration has to be avoided[4, 5], although i.v. injection could result in spleen enrichment of the vaccine, being favorable for DC targeting and DC-T cells communication for enhanced vaccination effect[5, 6]. To tackle the above outstanding issues, much effort has been devoted to developing carrier systems for mRNA delivery[6-9], and lipid-based nanomaterials are found to be most effective one. Effective packaging of mRNA by liposome-based materials

indeed provides protection against mRNA degradation and facilitates their cellular uptake. They also meet the requirement of cytosolic delivery for effective transfection to ensure desired antigen presentation[4, 10].

Other than effective antigen presentation, desired polarization of T helper cells and activation of effector T cells (CD 8+ T cells) also requires the presence of "danger signals", usually provided by adjuvant, the main function of which is to stimulate the maturation of dendritic cells[11]. In this regard, delivery of adjuvant and mRNA together is considered important. One shall note that timing is important in such delivery, as arrival of adjuvant in DCs earlier than the antigen would cause DC pre-maturation, inhibiting DC's capability of antigen uptake, and thus being detrimental to the vaccination[6]. On the other hand, choice of adjuvant is not random. Toll-like receptor (TLR) ligands have been known as one class of promising potent adjuvants for anticancer immunotherapy. In cancer vaccines, more polarized Th1 cell response is preferred, and it can be elicited by TLR3, TLR4, TLR7, TLR8 and TLR9 ligands[12, 13]. However, TLR8 ligand has been proposed to be expressed in humans, but not in mice, which may cause difficulties in animal models[13, 14]. TLR4 ligand is inefficient at eliciting CD8+ T cell response[12]. Thus, the TLR3, 7, and 9 ligands appear to be good adjuvant choices for cancer vaccine. TLR 7 ligand is particularly attractive for eliciting CD8+ T cell response[15-17] and inducing the release of type I interferons (IFNs) for effective T cell response and antitumor immunity[6, 16]. Unfortunately, the liposome-based carrier system only allows easy incorporation of lipid-similar adjuvants[16-18], but not other adjuvants, such as small molecules of TLR 7 ligand.

[a.] Department of Physics, The Chinese University of Hong Kong, Shatin, New Territories, Hong Kong
[b.] School of Biomedical Sciences, The University of Hong Kong, Hong Kong
Corresponding author
* Jiandong Huang, email: jdhuang@hku.hk
* Quan Li, email: liquan@phy.cuhk.edu.hk
[#] These authors contributed equally.

In the present work, we adopted a hybrid nanoparticle approach in designing the co-delivery system of mRNA and TLR7 adjuvant (Figure 1 (a)). A poly (lactic-co-glycolic acid) (PLGA)-core/lipid-shell nanoparticle was developed as the carrier. The adoption of PLGA core enabled efficient loading of the hydrophobic TLR7 adjuvant (gardiquimod in the present work), and the lipid shell allowed conjugation of mRNA. We demonstrated in the present work that co-delivery of mRNA and TLR7 adjuvant led to the effective antigen expression and DC activation *in vitro*. Intravenous administration of the hybrid nanovaccine resulted in enrichment of mRNA expression in spleen, and strong anti-tumor immune response *in vivo*. We further showed that the co-delivery (both spatially and temporally) of antigen and adjuvant enabled by the core/shell nanoparticle carrier is beneficial for tumor growth inhibition.

Results and Discussion

Design of hybrid particle for adjuvant loading together with mRNA

A lipid-coated PLGA (PLGA@lipid) hybrid carrier system was designed for co-delivery of mRNA and TLR7 adjuvant. PLGA, a biodegradable and biocompatible drug carrier, serves as an excellent candidate for encapsulating hydrophobic adjuvants (such as gardiquimod) and at the same time allowing liposome to reassemble onto its surface[19, 20]. PLGA nanoparticles with ~ 200 nm hydrodynamic size in diameter and a zeta potential of -20 mV were obtained first. The PLGA@lipid hybrid nanoparticles were made by lipid self-organization onto the as-synthesized PLGA nanoparticles with ~300 nm hydrodynamic size in diameter and ~32 mV zeta potential (size and zeta potential comparisons of pure PLGA and PLGA/lipid can be found in Table SI1). Transmission electron microscopy (TEM) image (Figure 1 (b)) showed the representative morphology of such a hybrid particle. The presence of dark ring (contributed by the negative staining of the lipid) suggested the core-shell structure of the hybrid system[21].

Adjuvant incorporation into the PLGA nanoparticles was realized by encapsulating gardiquimod into PLGA core via double emulsion. Gardiquimod-loaded PLGA also had hydrodynamic size ~ 200 nm in diameter and zeta potential about −20 mV (also listed in Table SI1). Both these values were similar to blank PLGA. Effective loading of gardiquimod into the PLGA nanoparticle was confirmed by the ultraviolet-visible (UV-VIS) absorption spectrum of gardiquimod-loaded PLGA (Figure 1 (c)). Characteristic absorption peak of gardiquimod at 333 nm was observed in such a sample. The loading efficiency of gardiquimod was estimated as 1.41 ± 0.03 % (details see experiments and Figure SI1).

Further incorporation of mRNA to the lipid layer on the gardiquimod-loaded hybrid nanoparticle increased the particle size to ~400 nm but with a rather narrow size distribution. The cationic lipid/mRNA charge ratio of 3:1 led to ~20 mV zeta potential of adjuvant-loaded hybrid-mRNA (Table SI1). The morphology of the mRNA loaded hybrid NP is similar to that of the hybrid nanoparticle without gardiquimod/mRNA loading (Figure 1 (b)). To find out whether mRNA can be successfully

conjugated onto the hybrid NPs, perylene (dye instead of gardiquimod) was encapsulated into the PLGA core and Cy5-mRNA was employed for imaging purpose. The obvious overlapping between the fluorescent signals of perylene at 450 nm in the polymeric core and Cy5-mRNA at 670 nm further confirmed the formation of hybrid-mRNA nanoparticles (Figure 1 (d)).
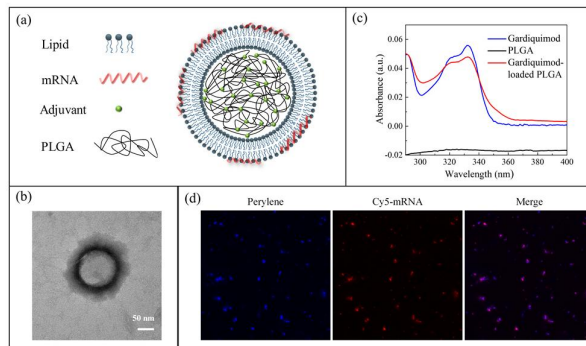

Figure 1 (a) Schematic illustration of the hybrid nanoparticles for co-delivery of mRNA and adjuvant. (b) TEM image disclosing the morphology of lipid-coated PLGA hybrid nanoparticle; (c) UV-VIS spectrum of gardiquimod-loaded PLGA, free gardiquimod and pure PLGA; (d) Fluorescence image showing the overlap between the fluorescence signal of the Cy5-mRNA and the perylene containing hybrid nanoparticles.

In vitro mRNA transfection of DCs by hybrid-mRNA nanoparticles

To induce an adaptive immune response, efficient transfection of mRNA-based vaccine should be realized in antigen presentation cells (APCs), e.g. dendritic cells (DCs)[22]. We therefore tested the mRNA transfection by feeding hybrid-mRNA nanoparticles to DC (the most efficient APC) in the presence of serum to mimic the conditions *in vivo*. The mRNA encoded with enhanced green fluorescence protein (EGFP) gene was used for both hybrid-mRNA and adjuvant-loaded hybrid-mRNA nanoparticles preparation. As shown in Figure 2 (a), little fluorescence signal was found in the control group (blank). Similar result was obtained in the dendritic cells fed with naked EGFP mRNA, being consistent with literature reports[23]. This is commonly ascribed to mRNA degradation in the presence of serum nucleases when no protection of mRNA is provided[22]. In contrast, strong fluorescence signal was observed in both hybrid-mRNA and adjuvant-loaded hybrid-mRNA treatment, indicating their improved transfection efficiency than naked mRNA. Quantitative results of the transfection efficiency in dendritic cells were obtained using flow cytometry (Figure 2 (b)). Here adjuvant-loaded hybrid-mRNA had the higher transfection efficiency of 29.05 ± 1.39% when compared to hybrid-mRNA (without adjuvant loading). This result indicated that the co-delivery of mRNA and adjuvant could improve the transfection efficiency. Overall, the transfection efficiency of adjuvant-loaded hybrid-mRNA was comparable to literature reports of lipid-based systems, in which transfection efficiency from 17% to 40% were obtained [24-27].
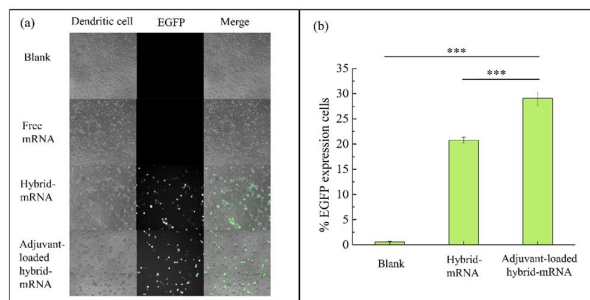
Figure 2 (a) Fluorescence images disclosing the EGFP mRNA transfection in DCs; (b) Flow cytometry analysis of EGFP mRNA transfection in DCs. Results are reported as mean ± SD, n=4, ***p < 0.001.

In vitro activation and antigen presentation of DCs by hybrid-mRNA nanoparticles

To determine whether gardiquimod-loaded hybrid mRNA NPs could activate dendritic cells, we treated the dendritic cells with PBS, hybrid-mRNA NPs (without gardiquimod loading), gardiquimod-loaded hybrid-mRNA NPs for 24h. The maturation of DCs was analyzed by measuring the expression level of the maturation surface markers CD80, CD86, and CD40. As shown in Figure 3, there was a significant upregulation in the expression levels of the activation markers CD80 (Figure 3 (a)), CD86 (Figure 3 (b)) and CD40 (Figure 3 (c)) after exposure to gardiquimod-loaded hybrid-mRNA NPs when compared to unstimulated cells (those of the PBS group are in the normal range[28]). The hybrid-mRNA NPs were also found to slightly increase the expression level of CD86 and CD40 (but not CD80), likely due to the self-adjuvant effect of mRNA[6]. Cells treated by gardiquimod-loaded hybrid-mRNA NPs showed a higher expression levels of surface markers when compared to hybrid-mRNA NPs, suggesting significantly promoted adjuvant effect after gardiquimod encapsulation in the hybrid nanocarriers.
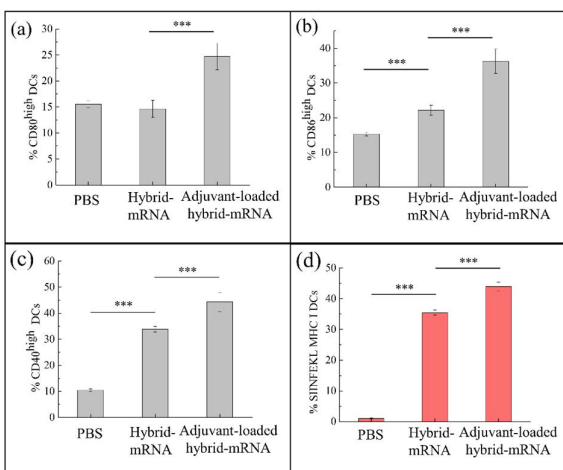

Figure 3 Flow cytometry analysis of CD80 (a), CD86 (b), and CD40 (c) expression on DCs, and SIINFEKL MHC I (d) expression on DCs. Results are reported as mean ± SD, n=4, **p < 0.01, ***p < 0.001.

Antigen presentation by DC is the key for antigen-specific T cell activation. Although both MHC I and II presentation are

involved in fully activating the antigen-specific CD8^{+} T cell, MHC I antigen expression is the most critical. We therefore examined the expression of ovalbumin (OVA)-derived MHC I-restricted peptide (SIINFEKL) in DCs after their treatment with different OVA-encoding mRNA complexes. Both treatment groups of hybrid-mRNA and adjuvant-loaded hybrid-mRNA have shown obvious MHC I SIINFEKL expression in DCs (Figure 3 (d)). In adjuvant-loaded hybrid-mRNA treatment group, the frequency of DCs expressing SIINFEKL MHC I was significantly higher than others.

In vivo transfection test

To further evaluate the transfection of mRNA *in vivo*, luciferase-encoding mRNA as a reporter gene was packaged with hybrid nanoparticles. The synthesized hybrid-mRNA and adjuvant-loaded hybrid-mRNA nanoparticles were respectively injected intravenously at the same dose of 8μg mRNA. After 18h following injection, the mice were imaged. Figure 4 (a) showed representative whole-body images of the injected mice. Both of hybrid-mRNA and adjuvant-loaded hybrid-mRNA showed intensified luminescence signal at the spleen. We then focused on comparing expression levels of them in the isolated organs (lungs and spleen). As shown in Figure 4 (b), luminescence signal was detected in both lungs and spleen in each sample. They had a similar expression level in the spleen, a major lymphoid organ where dense antigen presenting cells would enable efficient T cell priming and amplify T cell responses.
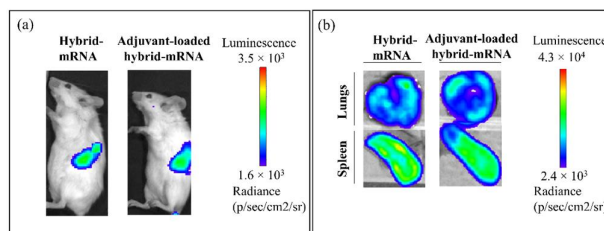

Figure 4 5-6-week-old BALB/c mice were administered with hybrid-luciferase mRNA and adjuvant-loaded hybrid-luciferase mRNA complexes and after 24 hours, mice were imaged using the IVIS spectrum *in vivo* imaging system (a) Representative whole body images of BALB/c mice after i.v. injection of hybrid-mRNA or adjuvant-loaded hybrid-mRNA (n=3). (b) Representative bioluminescence imaging of isolated organs (lungs and spleen) after i.v. injection of hybrid-mRNA or adjuvant-loaded hybrid-mRNA. Emitted photons were quantified as radiance (photons/s/cm^2/sr) represented by the color scale bars.

In vivo immune response

We next carried out *in vivo* investigation to find out whether the antigen-specific adaptive immune response could be induced by treatment with different OVA-encoding mRNA complexes. Different formulations were injected by intravenous administration at the equivalent dose of 8 μg OVA-encoding mRNA for five times. The exact injection time point is shown in Figure 5. After seven more days, the spleens of mice were harvested. Naïve T cells could differentiate to antigen-specific effector T cells in spleen upon immune response. We assessed the activation of antigen-specific effector T cell by using enzyme-linked immune absorbent spot (ELISPOT) assay to test the IFN-γ secretion originated from CD8^{+} T cells and CD4^{+} T cells. Large numbers of IFN-γ spots indicate more responsive T cells.

CD8^{+} T cells are key to killing tumors. To assess the OVA-specific CD8^{+} T cell response, immune cells isolated from spleens were re-stimulated with MHC I-restricted OVA peptide (SIINFEKL). As shown in Figure 5, the group of mice without immunization did not show any measurable number of IFN-γ spots. In contrast, all of mice vaccinated showed evident IFN-γ spots, indicating effective activation of OVA-specific CD8^{+} T cells. In different treatment groups, significantly higher amount of IFN-γ secretion was observed in adjuvant-loaded hybrid-mRNA, when compared to mice treated with hybrid-mRNA. This result demonstrated that adjuvant-loaded hybrid-mRNA induced stronger OVA-specific CD8^{+} T cells immune response than hybrid-mRNA.

Although CD4^{+} T cells are not involved directly to kill tumor, literature reported that simultaneous activation of CD4^{+} T cells promoted the priming of CD8^{+} T cells and induced a stronger anti-tumor response[29]. Here we also used OVA protein to re-stimulate splenocytes for measuring IFN-γ secretion mainly originated from OVA-specific CD4^{+} T cells, because OVA proteins internalized into endosome of DCs usually went through MHC II pathway for activation of CD4^{+} T cells[3]. Similar to the OVA-specific CD8^{+} T cell response, few IFN-γ spots were observed in the group of mice without treatment whereas obvious IFN-γ spots were obtained in the immunized mice, suggesting effective activation OVA-specific CD4^{+} T cells (Figure 5). When compared to hybrid-mRNA, the number of IFN-γ spots of adjuvant-loaded hybrid-mRNA were significantly higher than that of hybrid-mRNA. This result indicated that adjuvant-loaded hybrid-mRNA also had a stronger OVA-specific CD4^{+} T cell immune response than hybrid-mRNA (Figure 5). In evaluating the IFN-γ spots, significant contribution from other kinds of immune cells such as NK cells can be excluded, as they often lack antigen-specific cell surface receptors. We also compared group with re-stimulation and without re-stimulation. IFN-γ spot is not detectable in all groups without re-stimulation, suggesting that the effect of other immune cells on secreting IFN-γ spots was weak.
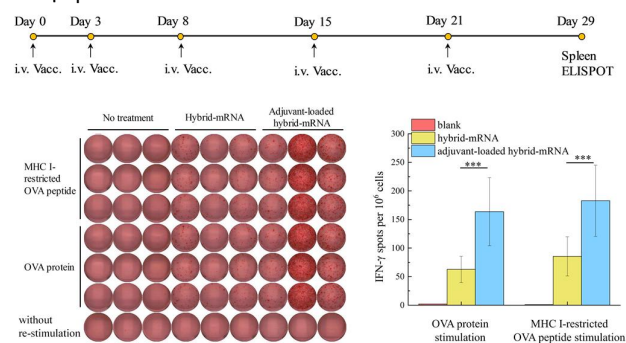

Figure 5 Vaccination scheme and IFN-γ ELISPOT assay of splenocytes after *ex vivo* restimulation with MHC-I restricted peptide (SIINFEKL) and OVA protein respectively on day29. 5-6-week-old C57BL/6J mice were intravenously administered with OVA-mRNA-hybrid and OVA-mRNA-adjuvant-loaded hybrid complex on day 0, 3, 8, 15 and 21. 8μg of OVA mRNA was used for each delivery and on day 29, and spleen of the mice was collected to perform ELISPOT ***p<0.001, analyzed by two-tailed unpaired Student's t-test. (n=3)

All treatment groups have shown simultaneous activation of OVA-specific CD4^{+} T cell and CD8^{+} T cell. Adjuvant-loaded

hybrid-mRNA vaccination elicited stronger immune response of both OVA-specific CD4^{+} T cell and CD8^{+} T cell than hybrid-mRNA, mainly due to the incorporation of adjuvant.

Tumor challenge

To evaluate the potential antitumor effect, we investigated both the protective and therapeutic efficacy of OVA-encoding mRNA vaccination by using B16-OVA melanoma tumor mice model. In addition to two formulations of hybrid-mRNA and gardiquimod-loaded hybrid-mRNA, one additional formulation using physical mixture of hybrid-mRNA and free gardiquimod was introduced to examine possible benefit gained from co-delivery (both spatially and temporally) of antigen and adjuvant. In the therapeutic model, mice were inoculated subcutaneously with B16-OVA melanoma cells first and vaccinated with different formulations at specific days shown in Figure 6 (a). From day 22 after the tumor inoculation, all groups began to show palpable tumors. Up to day 28 (the next day after the last immunization), only gardiquimod-loaded hybrid-mRNA treated group showed obviously delayed tumor growth when compared with control group. On day 30, all vaccinated groups have significantly smaller tumor size than the control group. When compared with hybrid-mRNA group, significant difference in tumor size was observed in gardiquimod-loaded hybrid-mRNA group (p < 0.0001) and hybrid-mRNA plus free gardiquimod group (p < 0.001) respectively. Representative tumor images in therapeutic model were included in the SI Figure 3(a). All mice in control, hybrid-mRNA and hybrid-mRNA plus free gardiquimod groups died within 40 days. Two mice in the gardiquimod-loaded hybrid-mRNA group without appearance of visible tumor survived for 50 days (the end of the study).
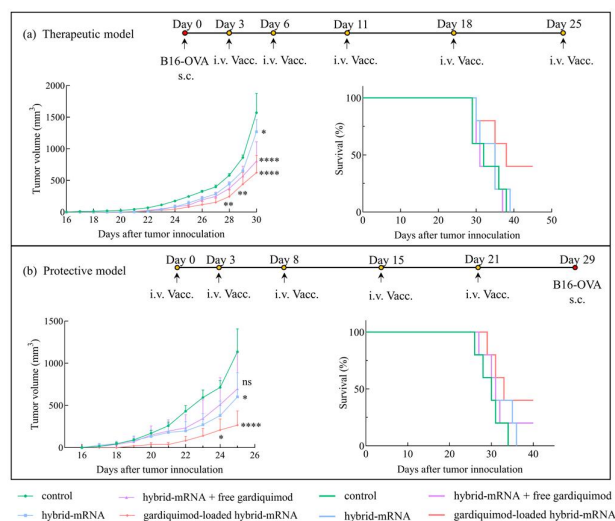

Figure 6 5-6-week-old C57BL/6J mice were challenged with B16-OVA tumor subcutaneously on their right flank and were then vaccinated with the OVA-encoding mRNA complexes for therapeutic vaccination while for prophylactic vaccination, mice were vaccinated first with OVA-encoding mRNA complexes and on day 29 they were challenged with the tumor subcutaneously. (a) Tumor growth and survival rate in therapeutic model. (b) Tumor growth and survival rate in protective model. In tumor growth curve, data are expressed as mean ± SEM, (ns, no significance, *p < 0.05, ***p < 0.001, compared with control group, two-way ANOVA with Bonferroni posthoc). (n=5)

In the protective model, mice were inoculated subcutaneously with B16-OVA melanoma cells seven days after the last immunization as illustrated in Figure 6 (b). On the day 19 after the tumor inoculation, gardiquimod-loaded hybrid-mRNA treated group started to show tumor growth, while control group and other treatment groups showed visible tumor from day 17. From day 24, gardiquimod-loaded hybrid-mRNA treated group showed significantly delayed tumor growth when compared with control group. On day 25, both gardiquimod-loaded hybrid-mRNA ($p < 0.0001$) and hybrid-mRNA ($p < 0.05$) groups have significantly smaller tumor size than those of the control group. In contrast, hybrid-mRNA plus free gardiquimod group did not show delayed tumor growth until day 25. Representative tumor images in protective model were shown in the SI Figure 3(b). The appearance of mice death in control and hybrid-mRNA groups started from day 26, and all of mice died within 36 days. The death of mice in hybrid-mRNA plus free gardiquimod and gardiquimod-loaded hybrid-mRNA groups occurred on day 27 and day 29 respectively. The respective survival rates in hybrid-mRNA plus free gardiquimod group and gardiquimod-loaded hybrid-mRNA group were 20% and 40% until day 40.

The gardiquimod-loaded hybrid-mRNA showed significantly delayed tumor growth in therapeutic as well as protective model. The survival rates of gardiquimod-loaded hybrid-mRNA were always higher than those of hybrid-mRNA plus free gardiquimod in both therapeutic and protective model, suggesting possible benefit from the spatial and temporal overlap of adjuvant and antigen co-delivery.

Conclusions

Co-delivery of mRNA and adjuvant was achieved by PLGA-core/lipid-shell hybrid nanoparticles system, where PLGA allowed the adjuvant incorporation in the core, and lipid shell loaded the mRNA via electrostatic interaction. Although the concept of multi-modality co-delivery has been proposed earlier[3, 30], and there have been many attempts to develop viable nanoplatforms for multi-functionality delivery[31], here we demonstrated co-delivery of mRNA and non-lipid like adjuvant for the first time. Potentially this design can be extended to other co-delivery system designs, as PLGA allows versatile type of adjuvants to be incorporated. Enhanced antigen expression and DC maturation were demonstrated in vitro when using such hybrid nanoparticles to co-deliver the mRNA and the adjuvant. Stronger antigen-specific immune response was obtained in intravenous administration of the hybrid nanovaccine containing both mRNA and TLR7 adjuvant than in those containing mRNA only. The anti-tumor effect of the hybrid nanovaccine was further demonstrated in both therapeutic and protective model employing B16-OVA. Spatial/temporal overlap of antigen and adjuvant co-delivery show some benefit in the present work, but the significance is likely to rely on the respective pharmacokinetic features of the specific adjuvant and nanoparticle used in the nanovaccine.

Experimental Sections

Mice and cell culture

C57BL/6J mice (5-6 weeks) and Balb/c mice 5-6 weeks) were obtained from laboratory animal unit in the University of Hong Kong. All animal experiments were performed following the protocols approved by committee of use of live animals in teaching and research of the University of Hong Kong.

To generate bone marrow-derived DCs (BMDCs), primary murine bone marrow cells were collected first. To start a culture of BMDCs, bone marrow cells were thawed and immersed in 6 mL RPMI 1640 medium (Life technology). The collected bone marrow cells (~10^7 cells) were culture in 75 cm^2 non-treated flask using 10 mL RPMI 1640 medium supplemented with 10% fetal bovine serum (FBS) (Life technology), 1% penicillin (Life technology), and 20 ng/mL granulocyte-macrophage colony-stimulating factor (GM-CSF) (In vivo gene) that was used to promote differentiation of the monocytes into BMDCs. Cells were maintained in humidified 5% CO_2 incubator at 37 °C. On day 3 of the culture, an additional 10 mL culture medium was added. After four more days, non-adherent and loosely adherent cells were harvested and used for the experiments as immature DCs.

Nanoparticles formulation

Liposomes composed of cationic lipid DOTAP (1, 2-dioleoyl-3-trimethylammonium-propane (chloride salt), Avanti Polar Lipids) and DOPE (1, 2-dioleoyl-sn-glycero-3-phosphoethanolamine, Avanti Polar Lipids) were synthesized by thin film rehydration method. Lipid solutions of DOTAP and DOPE were mixed in intended weight ratios of 3:1. The solvent was evaporated via nitrogen flow to form lipid films and the obtained lipid film was further dried under vacuum. The dry film was rehydrated with RNase-free water, which was shook gently overnight at 4 °C.

Dye-loaded poly (lactic-co-glycolic acid) PLGA nanoparticles were formed via oil/water (o/w) single emulsion method. Briefly, 100 mg PLGA and 1 mg perylene were co-dissolved in 2.5 mL mixed solvent of 1.5 mL dichloromethane (DCM) and 1 mL acetone. The mixture was added to 10 mL 5% (w/v) polyvinyl alcohol (PVA) solution dropwise under stirring. The solution was then sonicated for 6 min to generate emulsion. The organic solvent was further evaporated under stirring overnight at room temperature. Dye-loaded PLGA nanoparticles were collected and washed with distilled water by centrifugation and passed through 0.45 µm glass fiber filter (GE) to obtain uniform size. The nanoparticles were lyophilized and stored at 4 °C for later use. Blank PLGA nanoparticles were synthesized at the same method without addition of perylene. For gardiquimod loading, gardiquimod-loaded nanoparticles were also formed via double emulsion method for higher loading efficiency[32]. 2.5 mg sodium phosphate dibasic was dissolved in 500 µL 1% (w/v) PVA aqueous phase. This aqueous phase was added dropwise to the oil phase, which consisted of 30 mg PLGA and 3 mg gardiquimod co-dissolved in 2 mL chloroform. The mixture was sonicated by using ultrasonic tip for 6 min to generate the first emulsion. The w/o emulsion was further added to 8 mL 2% (w/v) PVA to form w/o/w emulsion and the following steps were also same as the synthesis of dye-loaded PLGA nanoparticles.

For PLGA@lipid hybrid nanoparticles formulation, PLGA nanoparticles were firstly resuspended in RNase-free water. PLGA nanoparticles suspensions were mixed with formulated liposomes solution at weight ratio of 0.75/1 (liposome/PLGA). The mixture was incubated for 30 min to obtain PLGA@lipid hybrid nanoparticles. mRNA-incorporated nanoparticles were synthesized following previous reference[6]. The complex was formed via electrostatic attraction between lipid and mRNA. So the N/P ratio (also defined as charge ratios) was calculated from the number of positive charges from amine groups of cationic lipid to those of negative charges from phosphodiester groups of mRNA. They are formed by diluting mRNA with H_2O and 1.5M NaCl and followed by adding various amounts of nanoparticles suspension to reach the selected N/P ratio of 3:1 at a final NaCl concentration of 150 mM.

Nanoparticles characterizations

Concentration and actual ratio of DOTAP and DOPE was determined by high performance liquid chromatography (HPLC) with an ultraviolet-visible detector at 205 nm referred to literature[33]. All size and zeta potential measurements were determined at 25 °C by dynamic light scattering (DLS) on a Nanosight at a diluted concentration. Each sample had three measurements with more than 10 runs.

The morphology of hybrid structure was disclosed by TEM. The TEM sample was stained with 2% phosphotungstic acid at 10 min for better imaging contrast. The fluorescence image disclosing the overlay of mRNA and hybrid NPs was measured by NIKON super resolution microscope.

For encapsulation and loading efficiency of mRNA estimation, the amount of unencapsulated mRNA was determined by using Nanodrop to measure the mRNA concentration in supernatant of hybrid-mRNA nanoparticles after ultracentrifugation. The encapsulation efficiency and loading efficiency was estimated around 91% and 4.6% respectively, which were based on the following respective equations, encapsulation efficiency = (1- weight of unencapsulated mRNA / weight of total mRNA added) × 100%, loading efficiency = weight of encapsulated mRNA / weight of hybrid-mRNA nanoparticles × 100%. For loading efficiency of adjuvant estimation, the sample of gardiquimod-loaded PLGA was dissolved in dimethyl sulfoxide (DMSO) and measured by UV-VIS spectra to obtain the absorption peak intensity of gardiquimod. Based on the standard equation, the amount of gardiquimod were acquired (Figure SI1). The loading efficiency (LE) is determined as LE = weight of gardiquimod / total weight of gardiquimod-loaded PLGA.

In vitro transfection test

Enhanced green fluorescence protein (EGFP)-encoding and Cy5-labled EGFP mRNA (Trilink) were employed to assemble with hybrid nanoparticles for in vitro transfection efficiency test. For transfection test of bone-marrow derived dendritic cells (BMDCs), BMDCs were transferred into 50 mL tube with culture medium (RPMI medium supplemented with 10% fetal bovine serum and 1% penicillin) permitting gas exchange. The hybrid-mRNA NPs and adjuvant-loaded hybrid-mRNA at the same amount of mRNA were respectively added to the cells. After 24 h incubation, cells were collected and washed with PBS

for flow cytometry or re-seeded in 96-well plate for fluorescence microscopy imaging.

In vitro maturation and antigen presentation

BMDCs were cultured in 50 mL tube. PBS (negative control), hybrid-mRNA NPs (without adjuvant, 59.5 μg/mL), and gardiquimod-loaded hybrid-mRNA NPs (59.5 μg/mL, equivalent to 0.2 μg/mL free gardiquimod) were added to each tube. After 24 h, BMDCs were collected and stained with CD40-PE, CD86-FITC, and CD80-PE Cy5. After additional washing steps, the cells were re-suspended in PBS to analyze DC maturation by flow cytometry using an S3e cell sorter. To assess MHC I antigen presentation, hybrid-mRNA, and gardiquimod-loaded hybrid-mRNA at the same dose of 5 μg mRNA-OVA were added to each tube. After 24 h, BMDCs were harvested and stained with anti-$OVA_{257-264}$ peptide bound to $H-2K^b$-PE antibody. The cells were washed and re-suspended in PBS to test OVA-specific MHC I presentation by flow cytometry. All data were analyzed by FlowJo software. Significance between two groups was determined by using unpaired two-tailed Student's t-test.

In vivo bioluminescence imaging

Firefly luciferase (Luc)-encoding mRNA-incorporated NPs were prepared for in vivo transfection test. Synthesized nanoparticles were injected intravenously at the same dose of 8 μg luciferase mRNA per mouse (Balb/c mice). After 18 h injection, mice were anesthetized first. Subsequently, luciferin was administered intraperitoneally in a volume of 200 μl (15 mg/ml) per mouse. After 3 min, bioluminescence images were acquired by the IVIS system with an exposure time of 5 min. For acquiring bioluminescence images of the separated organs, after 2 min luciferin injection, mice were sacrificed, and spleen and lungs were harvested.

In vivo immune response

C57BL/6J mice of age 5-6 weeks were grouped into three groups (n=3). Mice in control group remained untreated. Other three groups were immunized with different formulations. Hybrid-mRNA and gardiquimod-loaded hybrid-mRNA at the same dose of 8 μg mRNA-OVA were injected by intravenous on indicated time points, day0, day3, day8, day15 and day 22. Spleen of mice was harvested seven days after the last immunization for ELISPOT analysis. Splenocytes were extracted by milling spleen and then dealt with lysis buffer to remove red blood cells. 10^6 freshly isolated splenocytes were incubated with MHC I-restricted peptide (SIINFEKL) and OVA protein respectively in the microtiter plate coated with anti- IFN-γ antibody. After 18 hours incubation, the secondary antibody was added. The streptavidin binding was added after one more hour to wait for the spot's coloration. Finally, the IFN-γ spots were counted using an ELISPOT plate reader.

Tumor models

In tumor challenge, B16-OVA cell gifted by the lab of Professor Liu Zhuang was employed as the tumor model. In therapeutic model, B16-OVA cells (10^5) were inoculated subcutaneously on the right flank in C57BL/6J mice first. After three days, mice were immunized as the previous protocol. In protective model, C57BL/6J mice were immunized as the previous protocol first. After additional seven days, B16-OVA

cells (2×10^5) were inoculated subcutaneously. Once tumor was palpable, the tumor size was measured with a caliper. Tumor area was calculated using the equation width x length.
Statistical analysis

Results were presented as mean ± standard deviation (SD) or mean ± standard error of the mean (SEM). Unpaired two-tailed Student's t-test was used for comparisons of two groups. Two-way ANOVA with Bonferroni post-hoc test was used when both time and treatment were considered. Survival rate was analyzed with the log-rank test. Statistical analysis were performed with GraphPad Prism software. (*$p < 0.05$, **$p < 0.01$, ***$p < 0.001$, ****$p < 0.0001$)

Conflicts of interest

There are no conflicts to declare.

Acknowledgements

References

1. C. J. M. Melief, T. van Hall, R. Arens, F. Ossendorp and S. H. van der Burg, *J. Clin. Invest.*, 2015, 125, 3401-3412.
2. U. Sahin, K. Karikó and Ö. Türeci, *Nat. Rev. Drug Discov.*, 2014, 13, 759.
3. G. Zhu, F. Zhang, Q. Ni, G. Niu and X. Chen, *ACS Nano*, 2017, 11, 2387-2392.
4. K. A. Hajj and K. A. Whitehead, *Nat. Rev. Mater.*, 2017, 2, 17056.
5. S. Uchida, H. Kinoh, T. Ishii, A. Matsui, T. A. Tockary, K. M. Takeda, H. Uchida, K. Osada, K. Itaka and K. Kataoka, *Biomaterials*, 2016, 82, 221-228.
6. L. M. Kranz, M. Diken, H. Haas, S. Kreiter, C. Loquai, K. C. Reuter, M. Meng, D. Fritz, F. Vascotto, H. Hefesha, C. Grunwitz, M. Vormehr, Y. Hüsemann, A. Selmi, A. N. Kuhn, J. Buck, E. Derhovanessian, R. Rae, S. Attig, J. Diekmann, R. A. Jabulowsky, S. Heesch, J. Hassel, P. Langguth, S. Grabbe, C. Huber, Ö. Türeci and U. Sahin, *Nature*, 2016, 534, 396.
7. R. W. Malone, P. L. Felgner and I. M. Verma, *P. Natl. Acad. Sci.*, 1989, 86, 6077.
8. A. Akinc, M. Thomas, A. M. Klibanov and R. Langer, *J. Gene Med.*, 2005, 7, 657-663.
9. O. Boussif, Lezoualc, F. h, M. A. Zanta, M. D. Mergny, D. Scherman, B. Demeneix and J. P. Behr, *P. Natl. Acad. Sci.*, 1995, 92, 7297.
10. S. Rietwyk and D. Peer, *ACS Nano*, 2017, 11, 7572-7586.
11. Michael S. Goldberg, *Cell*, 2015, 161, 201-204.
12. R. L. Coffman, Sher, A., & Seder, R. A, *Immunity*, 2010, 33, 492-503.
13. Reed S G, Orr M T, Fox C B, *Nat. Med.*, 2013, 19, 1597.
14. Nuhn L, Vanparijs N, De Beuckelaer A, et al., *P. Natl. Acad. Sci.*, 2016, 113, 8098-8103.
15. F. Heil, H. Hemmi, H. Hochrein, F. Ampenberger, C. Kirschning, S. Akira, G. Lipford, H. Wagner and S. Bauer, *Science*, 2004, 303, 1526.
16. M. A. Oberli, A. M. Reichmuth, J. R. Dorkin, M. J. Mitchell, O. S. Fenton, A. Jaklenec, D. G. Anderson, R. Langer and D. Blankschtein, *Nano Lett.*, 2017, 17, 1326-1335.
17. R. Verbeke, I. Lentacker, L. Wayteck, K. Breckpot, M. Van Bockstal, B. Descamps, C. Vanhove, S. C. De Smedt and H. Dewitte, *J. Control. Release*, 2017, 266, 287-300.
18. R. Verbeke, I. Lentacker, K. Breckpot, J. Janssens, S. Van Calenbergh, S. C. De Smedt and H. Dewitte, *ACS Nano*, 2019, 13, 1655-1669.
19. S. Tan, X. Li, Y. Guo and Z. Zhang, *Nanoscale*, 2013, 5, 860-872.
20. A.-L. Troutier, L. Véron, T. Delair, C. Pichot and C. Ladavière, *Langmuir*, 2005, 21, 9901-9910.
21. L. Zhang, J. M. Chan, F. X. Gu, J.-W. Rhee, A. Z. Wang, A. F. Radovic-Moreno, F. Alexis, R. Langer and O. C. Farokhzad, *ACS Nano*, 2008, 2, 1696-1702.
22. K. A. Hajj, *Nat. Rev. Mater.*, 2017, 2, 17056.
23. X. Su, J. Fricke, D. G. Kavanagh and D. J. Irvine, *Mol. Pharm.*, 2011, 8, 774-787.
24. Verbeke R, Lentacker I, Wayteck L, et al., *J. Control. Release*, 2017, 266, 287-300.
25. Su X, Fricke J, Kavanagh D G, et al, *Mol. Pharm.*, 2011, 8, 774-787.
26. Irvine A S, Trinder P K E, Laughton D L, et al, *Nat. Biotech.*, 2000, 18, 1273.
27. Awasthi S, Cox R A, *Biotechniques*, 2003, 35, 600-604.
28. H. Kim, L. Niu, P. Larson, T. A. Kucaba, K. A. Murphy, B. R. James, D. M. Ferguson, T. S. Griffith and J. Panyam, *Biomaterials*, 2018, 164, 38-53.
29. K. Palucka and J. Banchereau, *Nat. Rev. Cancer*, 2012, 12, 265.
30. R. Kuai, L. J. Ochyl, K. S. Bahjat, A. Schwendeman and J. J. Moon, *Nat. Mater.*, 2016, 16, 489.
31. R. Xing, G. Liu, Q. Quan, A. Bhirde, G. Zhang, A. Jin, L. H. Bryant, A. Zhang, A. Liang, H. S. Eden, Y. Hou and X. Chen, *Chem. Commun.*, 2011, 47, 12152-12154.
32. H. Kim, D. Sehgal, T. A. Kucaba, D. M. Ferguson, T. S. Griffith and J. Panyam, *Nanoscale*, 2018, 10, 20851-20862.
33. Meyer O, Roch O, Elmlinger D, et al., *Euro. J. Pharm. Biopharm.*, 2000, 50, 353-356.